Climatic Change manuscript No.
(will be inserted by the editor)

Note that this is a non-peer reviewed EarthArXiv preprint

Implications of uncertain Antarctic ice sheet dynamics for managing future coastal erosion: a probabilistic assessment

Jasper Verschuur · Dewi Le Bars · Caroline A. Katsman · Sierd de Vries · Roshanka Ranasinghe · Sybren S. Drijfhout · Stefan G.J. Aarninkhof

Received: date / Accepted: date

Abstract Sea-level rise (SLR) can amplify the episodic erosion from storms and drive chronic erosion on sandy shorelines, threatening many coastal communities. One of the major uncertainties in SLR projections is the potential rapid disintegration of large fractions of the Antarctic ice sheet (AIS). Quantifying this uncertainty is essential to support sound risk management of coastal areas, although it is neglected in many erosion impact assessments. Here, we use the island of Sint Maarten as a case study to evaluate the impact of AIS uncertainty for future coastal recession. We estimate SLR-induced coastal recession using a probabilistic framework and compare and contrast three cases of AIS dynamics within the range of plausible futures. Results indicate that projections of coastal recession are sensitive to assumptions made on how AIS dynamics are incorporated into SLR projections and that underestimating the potential rapid mass loss from the AIS can lead to ill-informed coastal adaptation decisions.

J. Verschuur · C.A. Katsman · S. de Vries · S.G.J. Aarninkhof
Department of Hydraulic Engineering, Delft University of Technology, Stevinweg 1, 2628 CN Delft, The Netherlands
E-mail: jasperverschuur@gmail.com

J.Verschuur · D. Le Bars and S.S. Drijfhout
Royal Netherlands Meteorological Institute, Utrechtseweg 297, 3731 GA De Bilt, The Netherlands

S.S. Drijfhout
Institute for Marine and Atmospheric Research Utrecht, Department of Physics, Utrecht University, Princetonplein 5, 3584 CC Utrecht, The Netherlands

R. Ranasinghe
Department of Water Engineering, UNESCO-IHE, 3015 DA Delft, The Netherlands

R. Ranasinghe
Water Engineering and Management, University of Twente, 7500 AE Enschede, The Netherlands

R. Ranasinghe
Harbour, Coastal and Offshore Engineering, Deltares, 2600 MH Delft, The Netherlands

Keywords Coastal erosion · Sea-level rise · Probabilistics · Antarctica · Rapid disintegration

1 Introduction

Coastal zones have a large economic, environmental and aesthetic value, and are home to millions of people (McGranahan et al., 2007; Hallegatte et al., 2013). 24% of the world's sandy beaches are in a state of erosion (Luijendijk et al., 2018), and sea-level rise (SLR) will inevitably exacerbate the retreat of shorelines (Stive, 2004; FitzGerald et al., 2008; Ranasinghe and Stive, 2009; Hinkel et al., 2013; Anderson et al., 2015). Coastal managers are therefore now assigned with the daunting task of having to ensure more resilient coastal communities. The design of measures to mitigate coastal erosion (e.g. seawalls, nourishments, setback lines) hinge critically on SLR projections. These projections, however, have large inherent uncertainties, in particular associated with the potential rapid disintegration of the Antarctic Ice Sheet (AIS) from runaway feedbacks such as Marine Ice Sheet Instability (MICI) (Joughin et al., 2014; Ritz et al., 2015) and Marine Ice Cliff Instability (MISI) (Pollard et al., 2015; DeConto and Pollard, 2016; Oppenheimer and Alley, 2016).

Sandy shorelines are dynamic systems (Stive et al., 2002; Ranasinghe, 2016). During storms, elevated water levels together with extreme waves initiate episodic retreat of the shoreline, after which the shoreline recovers under fairweather conditions. Traditionally, to obtain predictions of storm driven beach erosion, a numerical model is forced with a design wave and surge condition (i.e. deterministic) to determine the resulting design storm erosion (Carley and Cox, 2003; Callaghan et al., 2009). Storm parameters (storm surge, wave height, wave period, wave angle, storm duration) are however stochastic in nature and covary with each other, making the aforementioned traditional approach sub optimal (Callaghan et al., 2008, 2009; Corbella and Stretch, 2012). SLR is expected to increase the frequency of extreme storm surges (Tebaldi et al., 2012; Buchanan et al., 2017), and will therefore contribute to an amplification of storm-induced erosion (McInnes et al., 2016; Ranasinghe, 2016).

On longer time-scales (decades-century), SLR will result in coastline recession. The 'Bruun Rule' is a commonly applied predictor of this process and governs the re-orientation of the active cross-shore profile landward and upward to maintain its equilibrium shape, thereby moving sand from onshore to offshore (Bruun, 1954). The 'Bruun Rule' is widely criticized with respect to its accuracy but is still routinely applied by practioners worldwide, mainly due to its ease of use (Cooper and Pilkey, 2004; Stive, 2004; Ranasinghe and Stive, 2009). Ranasinghe et al. (2012) introduced an alternative approach to model SLR-induced recession. This method deviates from the 'Bruun Rule' by coupling the morphodynamics of storm erosion and longer term recession using fundamental physical concepts. In addition, it has the advantage of providing probabilistic estimates of coastline recession. This methodology has also by now been applied in Australia (Ranasinghe et al., 2012), The Netherlands (Li et al., 2014b), Spain (Toimil et al., 2017), Sri Lanka (Dastgheib et al., 2018, in review) and France (Le Cozannet et al., 2018, in review), and further extended to quantify coastal erosion risk (Jongejan et al., 2016; Dastgheib et al., 2018, in review).

Given the billions of dollars of coastal assets at risk, effectively managing the coastal zone is essentially a risk-management issue (Cowell et al., 2006; Oppenheimer and Alley, 2016; Jongejan et al., 2016; Ranasinghe, 2016). Probabilistic projections of storm erosion and long-term recession is therefore a necessity to guide coastal managers in making risk-informed coastal zone management decisions. Management strategies should account for the uncertainty in SLR projections including potential rapid ice sheet dynamics. Therefore, alongside SLR projections provided by the Intergovernmental Panel on Climate Change (IPCC), high-end projections including recent understanding of the potential rapid mass loss from of the AIS (Le Bars et al., 2017; Kopp et al., 2017) should ideally be considered to better quantify the tail risk (i.e. events with low-probability but large consequences). In fact, tail risks may steer the mitigation alternatives (Kunreuther et al., 2013) and is essential for coastal managers that generally tend to be risk-averse (Hinkel et al., 2014). However, to date, the evaluation of SLR-induced erosion tail risk within a probabilistic framework is lacking in literature and is hence the main focus of this study.

Here, we evaluate how including different projections of AIS dynamics in SLR projections might affect the design values of coastal recession (by 2100). We consider three plausible future estimates (Section 2.2); one consistent with the latest report of the IPCC (AR5) (Church et al., 2013); a skewed distribution function of AIS dynamics based on Levermann et al. (2014); and a high-end scenario based on DeConto and Pollard (2016). Following the Probabilistic Coastline Recession (PCR) model introduced by Ranasinghe et al. (2012), here we use a probabilistic framework using synthetic storm time series (SSTS) (Section 2.3), an analytical erosion model and a shoreline prediction model (Section 2.4) to derive estimates of future storm erosion and recession (Section 3.2). The approach adopted here differs from prior PCR model applications in that here, for the first time, we introduce the implications of SLR uncertainty for coastal erosion management (Section 4.1).

2 Methods

2.1 Study area

The island of Sint Maarten is used as a case study to showcase the method. It has a rocky coastline with numerous embayed and pocket beaches. The tide is primarily diurnal with a tidal range rarely exceeding 20 cm (micro-tidal) (Kjerfve, 1981). The wave climate exhibits a seasonality with mean significant wave height between 1.5 and 2.0 m. Storms are triggered by locally generated waves, hurricane events during the North Atlantic hurricane season, and swell waves generated by intense mid-latitude storms during boreal winter (Jury, 2018).

Two beaches on the island are considered; Dawn Beach (DB) and Orient Bay (OB), which are embayed beaches that face the open ocean in the east (see Supplement Figure 1). Beaches are both reflective, without a complex dune structure or offshore bars and have typical grain size diameters (D_{50}) of 0.22 - 0.85 mm (Boon and Green, 1988).

2.2 Regional sea-level rise projections

Starting point of the probabilistic projections is the method of GMSL rise as in AR5 of the IPCC (Church et al., 2013) and extended by de Vries et al. (2014) and Le Bars et al. (2017). Here, only the modifications are presented with full details in the Supplement.

A rise in GMSL can be attributed to changes in mass loss from the Greenland ice sheet (GIS), AIS, glaciers and small ice caps (GIC) and land water (LW), and by thermal expansion and salinity changes of the ocean (ocean steric). Both ice sheets are further subdivided into a component that represents dynamic mass loss (dynamic processes at the ice-ocean boundary) and surface mass balance (mass changes due to accumulation and ablation). Regional SLR can differ from GMSL rise due to the self-gravitational and rotational effects of mass loss from the ice sheets, and changes in regional ocean dynamics and the inverse barometer (IB) effect (Slangen et al., 2014).

Three modifications are made relative to Church et al. (2013), namely (1) substitution of the AIS dynamics with two other estimates, (2) regional correlation between the ocean steric component and global mean surface temperature (GMST), and (3) including additional model uncertainty in the projections.

(1) In AR5, the AIS dynamics contribution is included by means of a uniform, scenario-independent, distribution function with median of 8 cm. This was based on Little et al. (2013), who extrapolated observed growth rate of discharge in part of West Antarctica and further quantified the uncertainty about future discharge from other drainage basins on the AIS. For the second case, results from Levermann et al. (2014) are used. Linear response theory is used to construct a probabilistic framework combining the results of five ice sheet numerical models to project ice discharge for varying basal melt scenarios (melt underneath the ice shelves due to an influx of warm ocean water). The use of linear response theory implies that self-amplifying effects such as MICI and MISI are assumed not to be dominant. The result for both RCPs is a skewed distribution function with the median close to the median value of Church et al. (2013), but with increased probability of larger mass loss. The third case includes the numerical model results of DeConto and Pollard (2016). Their projections of AIS contribution to end-century GMSL are hitherto the highest reported values from a numerical model. The numerical model has, apart from MISI feedback, the first parametrisation of hydrofracturing due to surface melting and ice-cliff structural failure, leading to the MICI feedback (Pollard et al., 2015). We follow the approach of Le Bars et al. (2017) on how to include these projections in the SLR framework.

(2) The ocean steric component and GMST are taken from the latest ensemble of global climate models; the Coupled Model Intercomparison Project Phase 5 (CMIP5). In AR5, the steric contribution to GMSL rise is assumed to be perfectly correlated with GMST ($\rho = 1.0$). However, for Sint Maarten, a local correlation coefficient of 0.4 is found from the CMIP5 models. The low local correlation can be well explained by the fact that steric effects are not only forced by GMST, but also depend on dynamical processes that are model dependent (Le Bars, 2018).

(3) Besides ocean steric effects and GMST, also ocean dynamics and IB are taken from the CMIP5 database. Climate models have common biases such as parametrisation of sub-grid physics and representation of the Atlantic meridional overturning

circulation (AMOC) (Wang et al., 2014; Maraun et al., 2017). The IPCC has therefore chosen to assign the 5-95 percentile range of climate model results a *likely range* (in IPCC typology this means 66-100% instead of exactly 90%). To account for the fact that the climate model range does not accurately represent the entire range of likely futures (Annan and Hargreaves, 2010), an additional model uncertainty is introduced, as done previously by Kopp et al. (2014) and Le Bars et al. (2017).

To construct regional SLR projections, the global projections of mass change are scaled to local scale using fingerprint values of Slangen et al. (2012, 2014). In this region, the fingerprint for the AIS has a value 15 to 30% above the global average, whereas GIS, GIC and LW are close to the global average (∼90-100%). This now results in regional SLR projections from 2006 to 2100 for the three cases of AIS dynamics and two representative concentration pathways (RCP); RCP4.5 and RCP8.5. Henceforth, we will abbreviate the different cases as IPCC, LEV14 and DP16.

2.3 Synthetic storm time series

SSTS allow sampling many plausible multi-variate storm time series (Callaghan et al., 2008; Li et al., 2014a; Wahl et al., 2016; Davies et al., 2017), which can be coupled to plausible SLR trajectories. The use of SSTS intrinsically assumes that the observations represent only one realization of potentially observed storm parameters instead of the full envelop of realizations. To derive the SSTS, we first create time series of storm parameters and extract storms from this. These storms are used to fit a stochastic model, from which random storm parameters can be sampled. Regional SLR trajectories can then be added to the storm surges to explore possible futures.

We extract data from satellite-based products that have a global coverage, which makes the approach generic and easily applicable in data-scarce environments.

2.3.1 Data retrieval

Storm parameters are here defined as a combination of wave and wind climate data (significant wave height H_s, peak wave period T_p, wave direction θ; wind speed u_{10}) and (storm) surge S. Time series of storm parameters are derived for a 25 year period (1993-2017) with 6h temporal resolution. H_s, T, θ and u_{10} are taken from the ERA-Interim reanalysis product (Dee et al., 2011). Data is extracted from an offshore location [18.125°N, 62.875°W] (OB) and [18.0°N, 62.875°W] (DB), where water depth is considered deep enough to assume linear (Airy) wave theory. A time series of S is constructed by adding up the astronomical tide η_a (FES2014, Carrere et al., 2015), atmospheric wind and pressure set-up η_{sur} (Mog2D-G, Carrère and Lyard, 2003), extra wind set-up η_{wis} and wave set-up η_{was} (Dean and Dalrymple, 2001). η_{was} requires information on breaking wave height H_b and depth h_b. To directly translate offshore wave conditions to breaking wave height, the predictive formula of Larson et al. (2010) is applied. This predictive formula essentially governs the wave energy flux conservation combined with Snell's law.

Storm events are extracted from the 25 year time series. Here, we define a storm as an offshore wave height threshold that, if surpassed, will result in morphological

change at the beach. This is supported by the fact that η_{was} dominates S (never less than 75-80%). Setting the threshold is however difficult, since we lack storm erosion data. To bridge this gap, satellite derived shoreline (SDS) positions from mid 2012 to early 2017 are obtained from Luijendijk et al. (2018). SDS are derived from satellite images that detect the shoreline using a shoreline detection algorithm. For the Sint Maarten beaches, the recurrence interval of satellite measurements is between 1 and 16 days over this period. From this, periods of shoreline erosion and accretion can be identified (Figure 1b), which show a clear seasonal cycle. We adopt an iterative approach of setting the wave height threshold, identifying storms and comparing the times that storms are identified with the instances that the shoreline is eroding. For both beaches, a threshold is set to 1.9 m that explains most instances that the shoreline is eroding (or already eroded). For Orient Bay, this is indicated by the grey lines in Figure 1 together with the corresponding values of H_s and S.

2.3.2 Implementation synthetic storm time series

From the storms identified in the time series, we extract storm parameters; peak H_s, peak S, the concordant T_P and θ of the peak H_s and the duration of the storm D above the threshold. To extract independent events, a 24h time interval time is set that has to be exceeded before a new storm is counted, following Li et al. (2014b). Moreover, storms are split into summer storms (April-September) and winter storms (November-March), to account for the seasonality that exist.

To model interdependencies between storm parameters, we use copulas. Copulas are very flexible, as they are independent of the underlying marginal distribution function of the variables (de Waal and van Gelder, 2005). A copula is fitted to the interdependencies $H_s - S$, $H_s - D$ and $H_s - T_p$ for both seasons, since the storm characteristics may stem from a different dependency structure. We test both elliptical copulas (Gaussian and t) and Archimedean copulas (Frank, Gumbel, Clayton), and perform a goodness-of-fit test based on *Cramèr-von Mises* $\mathscr{M}$ statistic (Genest et al., 2009). The t-copula is taken, which performs well and has the advantage of being elliptical, such that it can be extended to multiple dimensions easily. This copula is used to sample a four-dimensional set of the storm parameters (H_s, T_p, S, D), which are transformed back to the original scale using the inverse of the marginal distribution functions. For the marginals, a generalized Pareto distribution is used for H_s and D, whereas T_p and S are best represented using a generalized extreme value distribution. All fitted distribution functions pass the Chi-square goodness-of-fit test. Only wave angles within the range of incident angles are considered. θ can then be sampled independent of H_s from its empirical cumulative distribution function (ECDF). For the monthly storm frequency (F_s), a Poisson distribution is fitted to the monthly rate of storm occurrences (making yearly storm occurrence also Poisson distributed). From this, a random sample can be drawn for every month, with storms assigned a time position within a month (while maintaining again a 24h inter-arrival time between storms).

To constrain the samples within a physically realistic extent, a few boundaries are set (dashed line Figure 2). Observations show a maximum steepness of $s = 0.06$ between wave length (thus wave period) and a maximum duration of D = 350 h.

Additionally, following Wahl et al. (2016), the maximum wave period is fixed at 25 s, to avoid sampling waves that are being classified as infragravity waves (Munk, 1949). Stationary storm conditions is assumed for the SSTS. A trend analysis of (seasonal) storm parameters, similar to Wahl and Plant (2015), is performed. Results suggest that the seasonal cycle is slightly amplified (positive trend in winter, negative trend in summer) over the period 1993-2017. In contrast, climate models predict a small decline in wave and surge conditions for the future (Hemer et al., 2013; Vousdoukas et al., 2018). It is therefore chosen not to extrapolate this trend.

Now, many long time series of future storm events can be sampled. This is exemplified in Figure 2 where 10,000 sampled are generated and compared to the observations in blue (winter) and red (summer) together with the marginals. From here, it can be shown that the seasonal storms clearly stem from different underlying distribution functions. The dependency structure can be well represented using the *t*-copula, with the rank correlations (ρ_r) of the observations (black) compared to those of the seasonal copulas (red/blue).

SLR projections are constructed for the period 2006-2100, and so SSTS are also made for the same time period (95 years). SLR will gradually increase over the years and adds up to the *S* that is sampled by the copula (to enhance extreme *S*). A SLR trajectory is constructed by random sampling from the yearly ECDF of SLR. For instance, a 50th percentile trajectory consists of the 50th percentile values for every year. This SLR trajectory can then be added to the *S* values sampled for the corresponding years.

2.4 Storm erosion and shoreline position

Coastal morphological response to storm events and SLR is expressed by two parameters; the short-term retreat distance due to individual storms (*RD*) and the long-term coastal recession (*CR*).

To model *RD*, an analytical formula derived by Kriebel and Dean (1993) (henceforth KD93) is used that is fed by the storm parameters of the SSTS. The KD93 formulation has no calibration parameter and is therefore applied using the recommended settings (see Supplement). After a storm has eroded the beach, wave driven transport and aeolian processes will move sediment back to the beach and (partly) recover it before a new storm hits. With SLR, however, the magnitude of storm erosion will gradually increase and the beach does not have enough time to recover from extreme events (because extreme events are occurring more frequently). This drives a net sediment loss over the years, hence long-term *CR* of the coast. To forecast the shoreline position, the shoreline movements in between storm events also need to be quantified. We follow an approach similar to Ranasinghe et al. (2012) using a linear recovery rate, but deviate by introducing a simple state dependency (see Supplement). The state dependency is introduced since it is known that the rate of shoreline change is, apart from wave energy, determined by its antecedent position (Yates et al., 2009). We search for a representative recovery rate of the system that, on average, stabilizes the coast under a 500 yr simulation time in absence of SLR (storm forcing only). For Orient Bay, a representative recovery rate of 0.10 m day^{-1} is found, whereas for

Dawn Beach this recovery rate is 0.165 m day^{-1}. If SLR is now added in the simulations, the beach will gradually erode over time and the *CR* for a given year can be determined.

To validate the variability of the shoreline, the standard deviation of the detrended ECDF of SDS data and the 500 yr model run (without SLR) are compared. The standard deviation is a measure of the 'beach mobility' (Stive et al., 2002) and shows good agreement (Supplement).

2.5 Sampling and analysis

The above described methodology can be repeated multiple times. This is done as follows; (1) sample a SSTS together with a SLR pathway for 2006-2100, (2) calculate retreat distances due to storms and SLR, (3) forecast the shoreline behaviour using the recovery rate, (4) analyse the erosion hazard over the 95 year period, (5) repeat 10,000 times to obtain probabilistic estimates for all SLR cases.

For *RD*, a generalized Pareto distribution is fitted to the data and the return periods are calculated over the 2006-2100 period. The average shoreline position in 2100 is used to obtain *CR* estimates for 2100 compared to 2006.

3 Results

3.1 Regional sea-level rise

The results for IPCC, LEV14 and DP16 cases for 2100 compared to the 1986-2005 average are shown in Figure 3b&d. The median (95th percentile) value of DP16 is respectively 200 (266) cm for RCP8.5 and 108 (184) cm for RCP4.5. The skewed distribution function of the LEV14 case has a median value (95th percentile value) of 81 (134) cm for RCP8.5 and 57 (95) cm for RCP4.5. In contrast, the IPCC estimates reach 74 (111) cm and 54 (80) cm for the same percentiles and climate scenarios. Until 2060, results do not notably differ. Relative to GMSL rise, median SLR along the Sint Maarten coast will be 1.01-1.14 times larger.

3.2 Retreat distance and recession

Future return period of storm erosion over the years 2006-2100, including the 90% uncertainty range, are provided in Figure 4a-d. For comparison, the black line in Figures 4a-d is the baseline case without SLR. We define return periods as the average rate of occurrence of an event integrated over a given time span, here from 2006 till 2100. For instance, the 1/50 year will thus happen approximately twice over this period. For Orient Bay the return period of a 1/100 year retreat event is 1.67 (2.4) times higher for DP16 and around 1.4 (1.5) times higher for LEV14 and IPCC compared to the baseline under RCP4.5 (RCP8.5).

Figures 4e-f show the correlation between the SLR-value for a given year x and the 1/100 year retreat distance over the years (thus from 2006 to year x). The SLR

value sampled determines the trajectory taken. In case of a low correlation, the SLR trajectory sampled was apparently not a driving force for the 1/100 year erosion event (storm randomness dominates). Until 2060-2070, the correlation is still below 0.5 implying a moderate dependency. Thus, the increased frequency of extremer *S* will not alter the extreme value statistics much. For Orient Bay, the correlations in 2100 are close to 0.8-0.9 meaning that SLR is steering the extreme *RD* over the storm randomness, whereas for Dawn Beach this influence is less pronounced. The high correlation implies that there is an almost linear relation between SLR and *RD*. The difference between the two beaches can also be explained physically. Dawn Beach has a steeper beach slope and foreshore slope. According to Kriebel and Dean (1993), this yields a more reactive beach in terms of morphological response. This makes it less sensitive to an increase in *S* and more sensitive to the other storm parameters influencing *RD*.

Finally, *CR* for 2100 is summarized in Figure 5. First of all, Dawn Beach (Figure 5e&g) will experience larger *CR*, in line with the larger retreat distances, influenced by the morphological character of the Beach. Median *CR* values (black circle) range from 6-22 m for Dawn beach and 5-16 m for Orient Bay. However, the 1% exceedance probability (thin line upper panel) ranges from 13-45 m for Dawn Beach and 9-38 m for Orient Bay (Figure 5a&c). The lower value of the range corresponds to the IPCC case, whereas the upper range corresponds to the DP16 case, a 3.2-4.2 factor difference.

4 Discussion

4.1 Implications for decision-making

The main objective of this study was to quantify the sensitivity of future erosion estimates to different formulations of the AIS dynamics into SLR projections.

We evaluate this for retreat distance due to storms by considering the estimates of the IPCC for every return period and search for the relative return period for the other two cases (e.g. a 1/100 yr event has a value of 30 m for IPCC. 30m corresponds to a 1/x yr return period for LEV14). The result of this is displayed in Figure 4i-l. The dashed black line indicates perfect alignment between the cases with larger deviation from this line indicating larger difference. For example, a 1/100 yr erosion event for IPCC at Orient Bay (vertical black line) equals a 1/70 (1/60) event for LEV14 (solid blue line) and a 1/12 (1/2) event for DP16 (solid red line) for RCP4.5 (RCP8.5). Therefore, this event will occur 1.4-1.67 times as frequent for LEV14 and 8.3-50 times as frequent for DP16 over the same time span. For Dawn Beach, this effect is slightly less with relative return periods of 1/90 (1/80) for LEV14 and 1/35 (1/7) for DP16 given scenario RCP4.5 (RCP8.5). For larger return periods, the relative difference increases. Adopting the 95th percentile value instead of the median further increases the difference (dashed blue and red lines in Figure 4i-l), since the lines typically lie more downward. This is due to larger uncertainty in the SLR projections for LEV14 and DP16 compared to the IPCC, hence a larger uncertainty in the erosion estimates.

The same relative plots for coastal recession in 2100 compared to 2006 can be made, but now expressed in terms of exceedance probability. This is done in Figure 5b&d&f&h. Again, larger deviations from the perfect alignment (dashed black line) indicate larger differences (but now above this line). Large relative differences are found for the lower exceedance probabilities. For instance, the 1% exceedance probability for the IPCC case has a 3-4.5% exceedance probability for LEV14 and a 37-72% exceedance probability under DP16. This may be unacceptable in terms of risk faced by the coastal community. Besides, a given recession value for the IPCC case will be reached years ahead of 2100 in the other cases, which may alter the cost-efficiency of mitigation measures. We compare the recession values of the IPCC case in 2100 with the two other cases and search for the year where this value will be reached. This is done for a few exceedance probabilities and shown in Supplementary Figure 3. For DP16, the same exceedance probabilities for the IPCC case will be reached 20-25 years earlier, almost independent on the exceedance probability adopted. For LEV14, on the contrary, there is a dependency on the exceedance probability adopted, and the acceleration in terms of years is between 2-15 years.

4.2 Limitations

For the SLR projections, we do not consider RCP2.6 and RCP6.0. This is because RCP6.0 is comparable to RCP4.5, and RCP2.6 gives similar results of AIS dynamics in all three cases because rapid mass loss is not yet initiated. The AIS is expected to remain the main source of uncertainty in SLR projections, although ice sheet models have shown rapid improvements and can now move towards making refined future projections (Pattyn, 2018). Alternative ways to incorporate AIS uncertainty into projections could improve estimates, such as by using extra-probability theory (Le Cozannet et al., 2017) or expert elicitation (Bamber and Aspinall, 2013; Oppenheimer et al., 2016). In general, making SLR projections includes making non-trivial model design choices, i.e. the AIS dynamics, inclusion of extra model uncertainty, and the dependency structure between contributors. As it influences the results, hence the decision-making, transparency of such non-trivial choices is essential (discussed in Supplement). For instance, assumptions on the dependency between contributors primarily influences the tail estimates that are of interest (Le Bars, 2018).

In the stochastic model, we do not explicitly account for interannual and multidecadal variability in storm parameters, which may alter erosion risk (Wahl and Plant, 2015; Davies et al., 2017). Variability can often be linked to large scale atmospheric dynamics. We find, for example, a negative correlation between the monthly Niño3.4-index and monthly H_s ($\rho \sim$ -0.35).

Concerning the coastal impact model, the Kriebel and Dean (1993) formulation is suitable for first-order estimates, but not applicable in complex coastal settings or when higher accuracy estimates are required. Alternatively, other analytical formulas can be used (e.g. Larson et al., 2004), or replaced by a semi-empirical model (Callaghan et al., 2013). Because we lack of erosion data, we innovatively used satellite measurements to detect storms and set a threshold. Still, not all eroding moments could be detected in this way. This can be due to data inaccuracy in storm parameters,

due to accuracy of the SDS measurements that are on average 1-30 m (Hagenaars et al., 2018), or time mismatch between storms and measurements because the recurrence interval of the SDS is 1-16 days. Another point of discussion is the linear recovery rate of the beach. The values found are close to linear recovery rates mentioned in literature (summarized in Phillips et al., 2017) and identified in the SDS. In reality, however, dune/beach recovery is coupled to marine and aeolian processes (Cohn et al., 2018), making the recovery rate variable.

5 Conclusions

The aim of this study was to evaluate the implications SLR uncertainty for decision-making pertaining to future coastal zone management. A probabilistic approach is adopted where three cases of regional SLR projections are combined with synthetic storm time series and fed into a probabilistic storm erosion and shoreline prediction model.

We find that before 2070, SLR has only a moderate effect on the enhanced erosion from storms, because SLR driven increases in storm surge are not a dominant source of storm erosion until this time. However, after 2070, SLR starts to have a strong influence on storm erosion events and therefore model results diverge for different scenarios of SLR. Estimates of future erosion hazard tends to be prone to the assumptions made how to include the AIS dynamics into SLR projections. We estimate that return periods of future design storm erosion may differ up to a factor 50 under various AIS scenarios. In terms of longer term recession, estimates of exceedance probability (by 2100) differ by up to a factor 72 and a given recession value may therefore be reached 2-25 years ahead of 2100. In general, larger return periods and low-exceedance probabilities are relatively more sensitive to the various AIS dynamics scenarios; those who want to build in extra safety are more prone (relatively speaking) to a misconception about the level of safety.

The results of this study show that not accounting for AIS dynamics could lead to underestimating especially the low exceedance probability recessions, which are favoured by risk-averse coastal managers. Thus, precluding AIS uncertainty from SLR projections that feed into coastal impact assessments may lead to ill-informed adaptation decisions, alter the cost-efficiency of mitigation measures, and lead to potentially intolerable risk.

Further research in these topical areas could benefit from focussing on interdisciplinary work between the climate and coastal research communities to arrive at a better propagation of the uncertainties and eventually reduce it. Our approach could be extended by considering morphological uncertainties in all sources and sinks of the sediment budget (Dean and Houston, 2016), as well as providing insights on the natural variability of the shoreline on time scales spanning years to decades. This could be further stimulated by the development of reduced complexity models to model the SLR response in complex geomorphological settings, such as using a Bayesian Network (Lentz et al., 2016), or other surrogate models. Although we have focused primarily on the hazard component, risk management is a balance between risk and reward and the economic consequences of SLR-induced erosion need to be coupled

to this framework (Jongejan et al., 2016). A risk framework could further be used to evaluate potential engineering solutions (e.g. nourishments) (Hinkel et al., 2013).

Acknowledgements The authors would like to thank Arjen Luijendijk for providing the satellite derived shoreline positions of the Sint Maarten beaches. We further would like to acknowledge Ali Dastgheib for fruitful discussions during the research. RR is supported by the AXA Research fund and the Deltares Strategic Research Programme Coastal and Offshore Engineering.

References

Anderson TR, Fletcher CH, Barbee MM, Frazer LN, Romine BM (2015) Doubling of coastal erosion under rising sea level by mid-century in Hawaii. Nat Hazards 78(1):75–103, DOI 10.1007/s11069-015-1698-6

Annan J, Hargreaves J (2010) Reliability of the CMIP3 ensemble. Geophys Res Lett 37(L02703):1–5

Bamber J, Aspinall W (2013) An expert judgement assessment of future sea level rise from the ice sheets. Nat Clim Change 3:424–428

Boon J, Green MO (1988) Caribbean beach-face slopes and beach equilibrium profiles. Coast Eng 120:1618–1630

Bruun P (1954) Coast erosion and the development of beach profiles, beach erosion board technical memorandum. Tech. rep., U.S. Army Engineer Waterways Experiment Station. Vicksburg, MS

Buchanan M, Oppenheimer M, Kopp R (2017) Amplification of flood frequencies with local sea level rise and emerging flood regimes. Environ Res Lett 12(064009):1–7

Callaghan D, Nielson P, Short A, Ranasinghe R (2008) Statistical simulation of wave climate and extreme beach erosion. Coast Eng 55:375–390

Callaghan DP, Roshanka R, Andrew S (2009) Quantifying the storm erosion hazard for coastal planning. Coast Eng 56(1):90–93, DOI 10.1016/j.coastaleng.2008.10.003

Callaghan DP, Ranasinghe R, Roelvink D (2013) Probabilistic estimation of storm erosion using analytical, semi-empirical, and process based storm erosion models. Coast Eng 82:64–75, DOI 10.1016/j.coastaleng.2013.08.007

Carley J, Cox R (2003) A methodology for utilising time- dependent beach erosion models for design events. In: Proceedings of the 16th Australasian Coastal and Ocean Engineering Conference, Auckland, New Zealand

Carrère L, Lyard F (2003) Modeling the barotropic response of the global ocean to atmospheric wind and pressure forcing - Comparisons with observations. Geophys Res Lett 30(6):1997–2000, DOI 10.1029/2002GL016473

Carrere L, Lyard F, Cancet M, Guillot A (2015) FES 2014, a new tidal model on the global ocean with enhanced accuracy in shallow seas and in the Arctic region. EGU General Assembly Conference Abstracts 17:5481

Church J, Clark P, Cazenave A, Gregory J, Jevrejeva S, Levermann A, Merrifield M, Milne G, Nerem R, Nunn P, Payne A, Pfeffer W, Stammer D, Unnikrishan A (2013) Sea level change. in: Climate change 2013: The physical science basis. contribution of working group i to the fifth assessment report of the intergovernmental panel on climate change. Tech. rep., Cambridge University Press, Cambridge, United Kingdom and New York, NY, USA.

Cohn N, Ruggiero P, de Vries S, Kaminsky GM (2018) New Insights on Coastal Foredune Growth: The Relative Contributions of Marine and Aeolian Processes. Geophys Res Lett 45:4965–4973, DOI 10.1029/2018GL077836

Cooper J, Pilkey O (2004) Sea-level rise and shoreline retreat: time to abandon the bruun rule. Global Planet Change 43:157–171

Corbella S, Stretch D (2012) Predicting coastal erosion trends using non-stationary statistics and process-based models. Coast Eng 70:40–49

Cowell PJ, Thom BG, Jones RA, Everts CH, Simanovic D (2006) Management of Uncertainty in Predicting Climate-Change Impacts on Beaches. J Coast Res 221:232–245, DOI 10.2112/05A-0018.1

Dastgheib A, Jongejan R, Wickramanayake M, Ranasinghe R (2018) Regional scale risk-informed land-use planning using probabilistic coastline recession modelling and economical optimisation: East coast of Sri Lanka. J Mar Sci Eng in review

Davies G, Callaghan DP, Gravios U, Jiang W, Hanslow D, Nichol S, Baldock T (2017) Improved treatment of non-stationary conditions and uncertainties in probabilistic models of storm wave climate. Coast Eng 127(June):1–19, DOI 10.1016/j.coastaleng.2017.06.005

de Waal D, van Gelder P (2005) Modelling of extreme wave heights and periods through copulas. Extremes 8:345–356

Dean R, Dalrymple R (2001) Coastal processes with engineering applications. Cambridge University Press, Cambridge

Dean R, Houston J (2016) Determining shoreline response to sea level rise. Coast Eng 114:1–8

DeConto RM, Pollard D (2016) Contribution of Antarctica to past and future sea-level rise. Nature 531(7596):591–597, DOI 10.1038/nature17145

Dee D, Uppala S, Simmonds A, Berrisford P, Poli P, Kobayashi S, Andrae U, et al (2011) The era-interim reanalysis: configuration and performance of the data assimilation system. Q J Roy Meteorol Soc 137:553–597

FitzGerald D, Fenster M, andIV Buynevich BA (2008) Coastal impacts due to sea-level rise. Annu Rev Earth Planet Sci 36:601–647

Genest C, Rémillard B, Beaudoin D (2009) Goodness-of-fit tests for copulas: A review and a power study. Insur Math Econ 44(2):199–213, DOI 10.1016/j.insmatheco.2007.10.005

Hagenaars G, de Vries S, Luijendijk AP, de Boer WP, Reniers AJ (2018) On the accuracy of automated shoreline detection derived from satellite imagery: A case study of the sand motor mega-scale nourishment. Coast Eng 133:113–125, DOI 10.1016/j.coastaleng.2017.12.011

Hallegatte S, Green C, Nicholls RJ, Corfee-Morlot J (2013) Future flood losses in major coastal cities. Nat Clim Change 3(9):802–806, DOI 10.1038/nclimate1979

Hemer M, Fan Y, Mori N, Semedo A, Wang X (2013) Projected changes in wave climate from a multi-model ensemble. Nat Clim Change 3:471–476

Hinkel J, Nicholls R, Tol R, Wang Z, Hamilton J, Boot G, Vafeidis A, McFadden L, Ganopolski A, Klein R (2013) A global analysis of erosion of sandy beaches and sea level rise: an application of diva. Global Planet Change 111:150–158

Hinkel J, Lincke D, Vafeidis A, Perrette M, Nicholls R, Tol R, Marzeion B, Fettweis X, Ionescu C, Levermann A (2014) Coastal flood damage and adaptation costs under 21st century sea-level rise. PNAS 111(9):3292–3297

Jongejan R, Ranasinghe R, Wainwright D, Callaghan D, Reyns J (2016) Drawing the line on coastline recession risk. Ocean and Coastal Management 122:87–94

Joughin I, Smith BE, Medley B (2014) Marine Ice Sheet Collapse Potentially Under Way for the Thwaites Glacier Basin, West Antarctica. Science 344(6185):735–738,

DOI 10.1126/science.1249055
Jury M (2018) Characteristics and meteorology of atlantic swells reaching the caribbean. J Coast Res 34(2):400–412
Kjerfve B (1981) Tides of the caribbean. J Geophys Res 86(C5):4243–4247
Kopp R, Horton R, Little C, Mitrovica J, Oppenheimer M, Rasmussen D, Strauss B, Tebaldi C (2014) Probabilistic 21st and 22nd century sea-level projections at a global network of tide-gauge sites. Earth's Future 2:383–406
Kopp R, DeConto R, Bader D, Hay C, Horton R, Kulp S, Oppenheimer M, Pollard D (2017) Evolving understanding of antarctic ice-sheet physics and ambiguity in probabilistic sea-level projections. Earth's Future 5:1–17
Kriebel D, Dean R (1993) Convolution method for time-dependent beach-profile response. J Waterw Port Coast 119(2):204–226
Kunreuther H, Heal G, Allen M, Edenhofer O, Field CB, Yohe G (2013) Risk management and climate change. Nat Clim Change 3(5):447–450, DOI 10.1038/nclimate1740
Larson M, Erikson L, Hanson H (2004) An analytical model to predict dune erosion due to wave impact. Coast Eng 51:675–696
Larson M, Hoan L, Hanson H (2010) Direct formula to compute wave height and angle at incipient breaking. J Waterw Port Coast 136(2):119–122
Le Bars D (2018) Uncertainty in Sea Level Rise Projections Due to the Dependence Between Contributors. Earth's Future 6:1–17, DOI 10.1029/2018EF000849
Le Bars D, Drijfhout S, de Vries H (2017) A high-end sea level rise probabilitic projection including rapid antarctic ice sheet mass loss. Environ Res Lett 12(044013):1–10
Le Cozannet G, Manceau J, Rohmer J (2017) Bounding probabilistic sea-level projections within the framework of the possibility theory. Environ Res Lett 12(014012):1–11
Le Cozannet G, Bulteau T, Castelle B, Ranasinghe R, Wöppelmann G, Rohmer J, Bernon N, Idier D, Louisor J, Salas-y Melia D (2018) Uncertainties of sandy shoreline change projections as sea level rises. Sci Rep in review
Lentz EE, Thieler ER, Plant NG, Stippa SR, Horton RM, Gesch DB (2016) Evaluation of dynamic coastal response to sea-level rise modifies inundation likelihood. Nat Clim Change 6(7):696–700, DOI 10.1038/nclimate2957
Levermann A, Winkelmann R, Nowicki S, Fastook J, Frieler K, Greve R, Helmer H, Martin M, Meinshausen M, Mengel M, Payne A, Pollard D, Sato T, Timmermann R, Wang W, Bindschadler R (2014) Projecting antarctic ice discharge using response functions from searise ice-sheet models. Earth Syst Dynam 5:271–293
Li F, van Gelder P, Ranasinghe R, Callaghan D, Jongejan R (2014a) Probabilistic modelling of extreme storms along the Dutch coast. Coast Eng 86:1–13, DOI 10.1016/j.coastaleng.2013.12.009
Li F, van Gelder P, Vrijling J, Callaghan D, Jongejan R, Ranasinghe R (2014b) Probabilistic estimation of coastal dune erosion and recession by statistical simulation of storm events. Appl Ocean Res 47:53–62, DOI 10.1016/j.apor.2014.01.002
Little C, Urban N, Oppenheimer M (2013) Probabilistic framework for assessing the ice sheet contribution to sea level change. PNAS 110(9):3264–3269

Luijendijk A, Hagenaars G, Ranasinghe R, Baart F, Donchyts G, Aarninkhof S (2018) The state of the world's beaches. Sci Rep 8(6641):1–11

Maraun D, Shepherd TG, Widmann M, Zappa G, Walton D, Gutiérrez JM, Hagemann S, Richter I, Soares PM, Hall A, Mearns LO (2017) Towards process-informed bias correction of climate change simulations. Nat Clim Change 7(11):764–773, DOI 10.1038/nclimate3418

McGranahan G, Balk D, Anderson B (2007) The rising tide: assessing the risks of climate change and human settlements in low elevation coastal zones. Environ Urban 19(1):17–37

McInnes KL, White CJ, Haigh ID, Hemer MA, Hoeke RK, Holbrook NJ, Kiem AS, Oliver EC, Ranasinghe R, Walsh KJ, Westra S, Cox R (2016) Natural hazards in Australia: sea level and coastal extremes. Climatic Change 139(1):69–83, DOI 10.1007/s10584-016-1647-8

Munk WH (1949) Surf beats. Transaction American Geophysical Union 30(6)

Oppenheimer M, Alley R (2016) How high will the seas rise? Science 354(6318):1375–1376

Oppenheimer M, Little CM, Cooke RM (2016) Expert judgement and uncertainty quantification for climate change. Nat Clim Change 6(5):445–451, DOI 10.1038/nclimate2959

Pattyn F (2018) The paradigm shift in Antarctic ice sheet modelling. Nat Comm 9(1):2728, DOI 10.1038/s41467-018-05003-z

Phillips MS, Harley MD, Turner IL, Splinter KD, Cox RJ (2017) Shoreline recovery on wave-dominated sandy coastlines: the role of sandbar morphodynamics and nearshore wave parameters. Mar Geol 385:146–159, DOI 10.1016/j.margeo.2017.01.005

Pollard D, DeConto RM, Alley RB (2015) Potential Antarctic Ice Sheet retreat driven by hydrofracturing and ice cliff failure. Earth Planet Sci Lett 412:112–121, DOI 10.1016/j.epsl.2014.12.035

Ranasinghe R (2016) Assessing climate change impacts on open sandy coasts: A review. Earth Sci Rev 160:320–332, DOI 10.1016/j.earscirev.2016.07.011

Ranasinghe R, Stive MJF (2009) Rising seas and retreating coastlines. Climatic Change 97(3-4):465–468, DOI 10.1007/s10584-009-9593-3

Ranasinghe R, Callaghan D, Stive M (2012) Estimating coastal recession due to sea level rise: beyond the bruun rule. Climatic Change 110:561–574

Ritz C, Edwards T, Durand G, Payne A, Peyaud V, RCA H (2015) Potential sea-level rise from antarctic ice-sheet instability constrained by observations. Nature 528:115–129

Slangen A, Carson M, Katsman C, van der Wal R, Kohl A, Vermeersen L, DStammer (2014) Projecting twenty-first century regional sea-level changes. Climatic Change 124(1-2):317–332

Slangen ABA, Katsman CA, van de Wal RSW, Vermeersen LLA, Riva REM (2012) Towards regional projections of twenty-first century sea-level change based on IPCC SRES scenarios. Clim Dynam 38(5-6):1191–1209, DOI 10.1007/s00382-011-1057-6

Stive MJ, Aarninkhof SG, Hamm L, Hanson H, Larson M, Wijnberg KM, Nicholls RJ, Capobianco M (2002) Variability of shore and shoreline evolution. Coast Eng

47(2):211–235, DOI 10.1016/S0378-3839(02)00126-6

Stive MJF (2004) How important is global warming for coastal erosion? Climatic Change 64(1):27–39, DOI 10.1023/B:CLIM.0000024785.91858.1d

Tebaldi C, Strauss BH, Zervas CE (2012) Modelling sea level rise impacts on storm surges along US coasts. Environ Res Lett 7(1), DOI 10.1088/1748-9326/7/1/014032

Toimil A, Losada IJ, Camus P, Díaz-Simal P (2017) Managing coastal erosion under climate change at the regional scale. Coast Eng 128(July):106–122

Vousdoukas MI, Mentaschi L, Voukouvalas E, Verlaan M, Jevrejeva S, Jackson LP, Feyen L (2018) Global probabilistic projections of extreme sea levels show intensification of coastal flood hazard. Nat Comm 9(1):2360, DOI 10.1038/s41467-018-04692-w

de Vries H, Katsman C, Drijfhout S (2014) Constructing scenarios of regional sea level change using global temperature pathways. Environ Res Lett 9(115007):1–8

Wahl T, Plant NG (2015) Changes in erosion and flooding risk due to long-term and cyclic oceanographic trends. Geophys Res Lett 42(8):2943–2950, DOI 10.1002/2015GL063876

Wahl T, Plant N, Long J (2016) Probabilistic assessment of erosion and flooding risk in the northern gulf of mexico. J Geophys Res C Oceans 121:3029–3042

Wang C, Zhang L, Lee SK, Wu L, Mechoso CR (2014) A global perspective on CMIP5 climate model biases. Nat Clim Change 4(3):201–205, DOI 10.1038/nclimate2118

Yates ML, Guza RT, O'Reilly WC (2009) Equilibrium shoreline response: Observations and modeling. J Geophys Res C Oceans 114(9):1–16, DOI 10.1029/2009JC005359

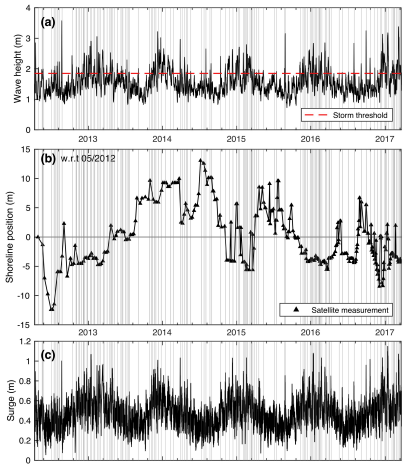

Fig. 1 (a) Time series of H_s together with the storm threshold of 1.9 m (red line). (b) Satellite derived shoreline (SDS) positions of Orient Bay with linear interpolation between SDS measurements (triangles). The shoreline position is relative to the position on March, 2012. (c) Time series of S. The grey line in (a-c) indicate the onset of the storm events as identified by the threshold.

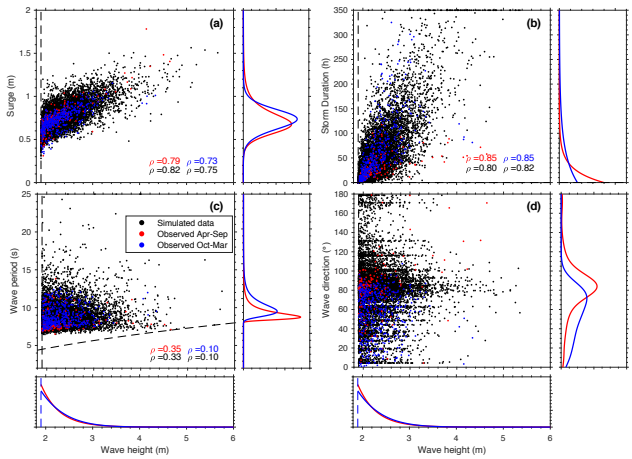

Fig. 2 (a) Scatterplot of observed variables H_s and S for both winter months (blue) and summer months (red). The black dots show a 10,000 random sample using the copulas. In the boxes, The univariate marginal distribution functions are shown in the boxed. Spearman rank correlation (ρ_r) of the seasonal observations (red and blue) are compared to those obtained from the sampled copula (black). (b) same as (a) but for H_s-D. (c) same as (a) but for H_s-T_p. Black dashed line indicate the steepness limit set ($s = 0.06$). (d) Same as (a) but for $H_s$and θ that is sampled independently from the empirical cumulative distribution function (no correlation compared).

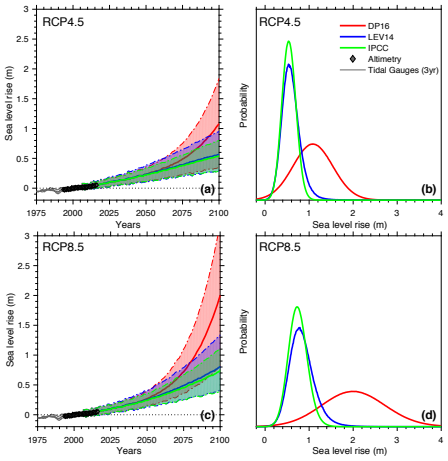

Fig. 3 (a) Regional SLR projections from 2006 to 2100 for RCP4.5. Grey line indicate 3 year running average of tidal gauge stations (PSMSL) and grey diamonds recent altimetry data (*aviso.altimetry.fr*) for the Caribbean. (b) PDFs of 2100 regional SLR compared to 1986-2005 under RCP4.5. (c-d) same as (a-b) but for RCP8.5.

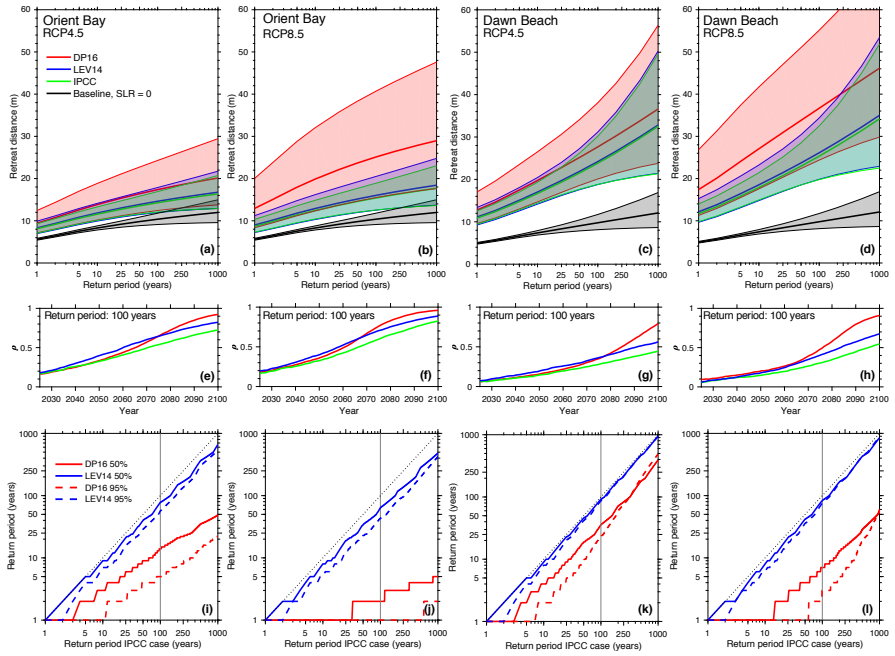

Fig. 4 (a) Return periods of retreat distance due to storm events over the period 2006-2100 for Orient Bay under RCP4.5. Median value (solid line) together with the 90% uncertainty (shaded area). (b) same as (a) but under RCP8.5. (c-d) same as (a-b) but for Orient Bay. (e) Correlation between sample year x SLR and the calculated 1/100 year retreat distance over 2006-year x for Orient Bay under RCP4.5. (f) same as (e) but under RCP8.5. (g-h) same as (e-f) but for Dawn Beach. (i) Comparison between return periods of retreat distance from storm events under the IPCC scenario and the DP16 (red) and LEV14 (blue) scenario. The dashed black line indicate perfect agreement (no difference). (j-k) same as (i) but for different RCP and different beach.

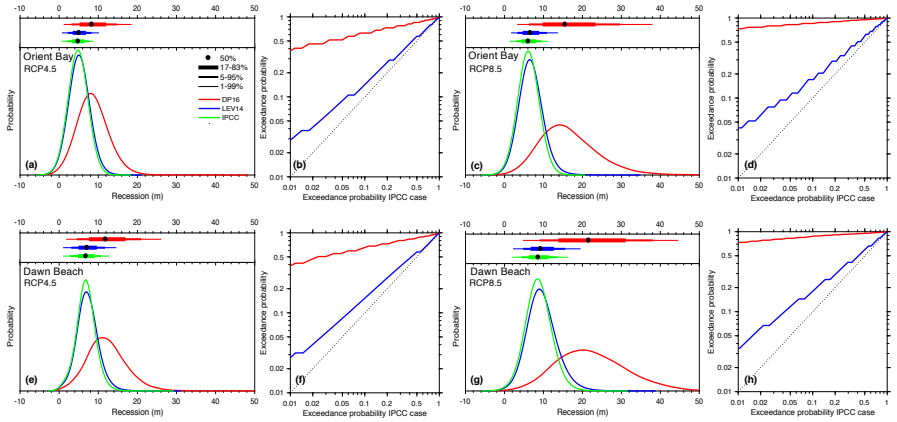

Fig. 5 (a) PDFs of 2100 recession values compared to 2006 for Orient Bay under RCP4.5. In the top panel, the median is shown together with the 66%, 90% and 98% uncertainty range. (b) Comparison between exceedance probabilities of recession values in 2100 compared to 2006 under the IPCC scenario and the DP16 (red) and LEV14 (blue) scenario. The dashed black line indicate perfect agreement (no difference). (c-d) same as (a-b) but under RCP8.5. (e-h) same as (a-d) but for Dawn Beach.